ACS OMEGA

Article

Cite This: ACS Omega 2018, 3, 14650−14664

http://pubs.acs.org/journal/acsodf

Cell-Selective Pore Forming Antimicrobial Peptides of the Prodomain of Human Furin: A Conserved Aromatic/Cationic Sequence Mapping, Membrane Disruption, and Atomic-Resolution Structure and Dynamics

Sheetal Sinha,[†,‡,§] Munesh Kumar Harioudh,[⊥] Rikeshwer P. Dewangan,[⊥] Wun Jern Ng,[∥] Jimut Kanti Ghosh,[⊥] and Surajit Bhattacharjya*[,†]

[†]School of Biological Sciences, Nanyang Technological University, 60 Nanyang Drive, Singapore 637551

[‡]Advanced Environmental Biotechnology Centre, Nanyang Environment and Water Research Institute, Nanyang Technological University, 1 Cleantech Loop, Singapore 637141

[§]Interdisciplinary Graduate School and [∥]Environmental Bio-Innovation Group (EBiG), School of Civil and Environmental Engineering, Nanyang Technological University, 50 Nanyang Avenue, Singapore 639798

[⊥]Molecular and Structural Biology Division, CSIR-Central Drug Research Institute, Sector 10, Jankipuram Extension, Sitapur Road, Lucknow 226 031, India

Supporting Information

ABSTRACT: Antimicrobial peptides are promising molecules in uprising consequences of drug-resistant bacteria. The prodomain of furin, a serine protease, expressed in all vertebrates including humans, is known to be important for physiological functions. Here, potent antimicrobial peptides were mapped by extensive analyses of overlapping peptide fragments of the prodomain of human furin. Two peptides, YR26 and YR23, were active against bacterial cells including MRSA-resistant *Staphylococcus aureus* and *Staphylococcus epidermis* 51625. Peptides were largely devoid of hemolytic and cytotoxic activity. Bacterial cell killing occurred as a result of the disruption of the permeability barrier of the lipopolysaccharide (LPS)-outer membrane and fragmentation of LPS into small micelles. Furthermore, antibacterial peptides specifically interacted with the negatively charged lipids causing membrane leakage and fusion. The YR26 peptide in sodium dodecyl sulfate micelles demonstrated a long-helix-turn-short-helix structure exhibiting restricted backbone motions. The cell-selective activity of the furin peptides and their unique mode of action on membranes have a significant potential for the development of therapeutics.

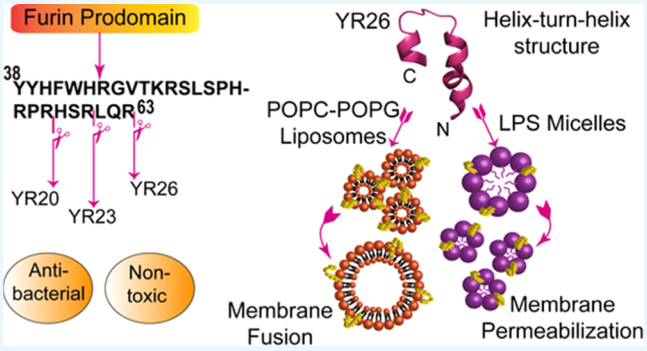

INTRODUCTION

Antibiotic-resistant bacteria are the eminent global health threat that may kill over 30 million people by 2050.[1−3] In the United States alone, annually over 2 million population are estimated to be infected by drug-resistant bacteria.[4] Infections caused by multidrug-resistant ESKAPE pathogens (*Enterococcus faecium*, *Staphylococcus aureus*, *Klebsiella pneumoniae*, *Acinetobacter baumannii*, *Pseudomonas aeruginosa*, and *Enterobacter* species) could be untreatable.[5,6] On the face of escalating drug resistance, a high attrition rate has slowed the discovery of new antibiotics that often uses old drug as starting candidates.[7,8] Only three antibiotics were approved by the food and drug administration (FDA) of the United States in past few years.[7,8] Although the pipeline of small molecule antibiotics are becoming limiting, there has been a pronounced interest in developing antimicrobial peptides (AMPs) to enrich antibiotic resources.[9−13] AMPs, also known as host defense peptides, exist in all life forms encompassing bacteria, plants, invertebrates, and vertebrates.[14−16] Naturally occurring cationic AMPs in animals constitute an integral part of the innate and also adaptive immune defense systems.[17−19] These amphipathic AMPs target the negatively charged lipid of the membrane of microbes by passing the recognition of any surface receptor. The membrane permeabilization mechanism of AMPs involves disruption of the permeability barrier of the outer membrane lipopolysaccharide (LPS) or cell wall followed by pore formation in the lipid bilayer.[20−25] The membranolytic activity of AMPs would cause a challenge toward developing drug resistance in bacteria.[20−25] Non-membranolytic AMPs with an alternate mode of action that

Received: August 3, 2018
Accepted: September 26, 2018
Published: November 1, 2018

DOI: 10.1021/acsomega.8b01876
ACS Omega 2018, 3, 14650−14664

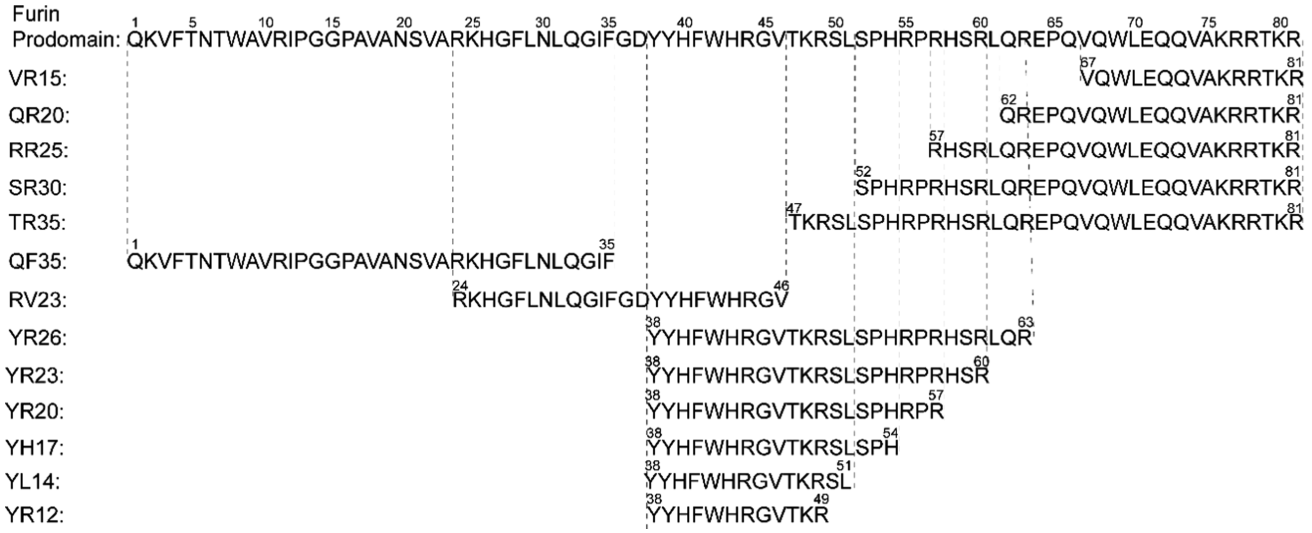

Figure 1. Mapping sequence of the prodomain of furin and its various fragments for antimicrobial peptides.

Table 1. Minimum Inhibitory Concentration to Screen Various Prodomain Truncations[a]

	Gram-negative (μM)				Gram-positive (μM)			
	EC	PA	SE	KP	BS	SA	SP	EF
VR15	>100	>100	>100	>100	>100	>100	>100	>100
QR20	>100	>100	>100	>100	>100	>100	>100	>100
RR25	>100	>100	>100	>100	>100	>100	>100	>100
SR30	>100	>100	>100	>100	>100	>100	>100	>100
TR35	>100	>100	>100	>100	>100	>100	>100	>100
YR26	2	4	4	2	2	4	4	4
RV23	4	>100	>100	>100	>100	>100	>100	>100
QF35	20	>100	>100	>100	>100	>100	>100	>100

[a]MIC (μM) against EC: *E. coli*; PA: *P. aeruginosa*; SE: *Salmonella enterica*; KP: *K. pneumoniae*; SA: *S. aureus*; BS: *Bacillus subtilis*; SP: *Streptococcus pyogenes*; and EF: *E. faecalis*.

target intracellular macromolecular proteins or DNA are also described.[26−28]

In humans, host defense proteins and peptides play eminent roles in eliminating invading pathogens as a part of innate immunity.[29,30] The antimicrobial peptide database (APD) lists a total of 123 antimicrobial peptides and proteins.[31] Human AMPs, defensins (α and β), cathelicidin LL37, histatins, and dermcidin, are expressed in variety of tissues, cells, and eccrine systems including skin, eyes, sweat, lungs, intestine lining, and urinary bladder.[32−36] Several large human proteins e.g., multiple RNases, lysozyme, chemokines, and psoriasin are known to be possessing antimicrobial activity.[29,37,38] Apart from the bona fide AMPs and antimicrobial proteins, peptide fragments of native proteins of human have demonstrated antimicrobial activity.[39−42] Prodomains of proteases are cleaved during the maturation or activation of the enzymes. The proteolysis-derived peptide fragments may display antimicrobial activity in host defense systems.[43−45] Furin, a serine proprotein convertase, is widely expressed in numerous cells and remains responsible for processing precursor proteins in the constitutive secretory pathways.[46,47] Furin can activate bacterial and viral toxin proteins and is a target for drug development.[46,47] The 81-residue furin prodomain undergoes proteolytic cleavages during the activation of the zymogen.[46,47] In solution, furin prodomain assumes partially folded molten globule like conformations or helical structures.[48,49] Several recent studies demonstrated important cellular activities of the prodomain of furin including anticancer activity.[50−54]

In this work, we demonstrate that peptides derived from the central cationic/aromatic rich region of the furin prodomain delineated potent antibacterial activity against Gram-negative, Gram-positive, and MRSA-resistant *Staphylococcus* strains. These antimicrobial peptides were low in hemolytic and cytotoxic activity to mammalian cells. As a mode of action, potent peptides interacted especially with the negatively charged lipids in model membranes, disrupted outer membrane LPS, neutralized surface charge, and permeabilized bacterial cell membrane. The atomic-resolution structure of a 26-residue long active peptide, termed YR26, was determined by NMR in the presence of negatively charged sodium dodecyl sulfate (SDS) micelles. The structure revealed a novel fold consisting of an N-terminal long helix followed by a tight turn and C-terminus short helix. This study underscores the significance of the prodomain of proteases and proprotein convertases in generating cell-specific antimicrobial peptides that can be potentially used for the development of antibiotics that are nontoxic to human.

RESULTS

Screening of Peptide Fragments Derived from the Prodomain of Furin for Antimicrobial Activity. The primary structure of the prodomain of furin is rich in basic amino acids (pI ∼ 11.93) with a high preponderance of

DOI: 10.1021/acsomega.8b01876
ACS Omega 2018, 3, 14650−14664

Table 2. Minimum Inhibitory Concentration (MIC, in μM) of Deletion Analogs of YR26[a]

	Gram-negative (μM)				Gram-positive (μM)					
	EC	PA	SE	KP	BS	SA	SP	EF	SA BBA-44	SE*
YR12	40	40	40	40	40	30	70	30		
YL14	30	60	80	70	60	80	>100	70		
YH17	30	>100	>100	>100	>100	>100	>100	>100		
YR20	6	8	8	6	6	6	15	6	>30	>30
YR23	4	4	4	2	4	4	6	4	6	6
YR26	2	4	4	2	2	4	4	4	6	6

[a]EC: *E. coli*; PA: *P. aeruginosa*; SE: *S. enterica*; KP: *K. pneumoniae*; SA: *S. aureus*; BS: *B. subtilis*; SP: *S. pyogenes*; EF: *E. faecalis*. SA BBA-44: MRSA-resistant *S. aureus*, and SE*: MRSA-resistant *Staphylococcus epidermis* 51625.

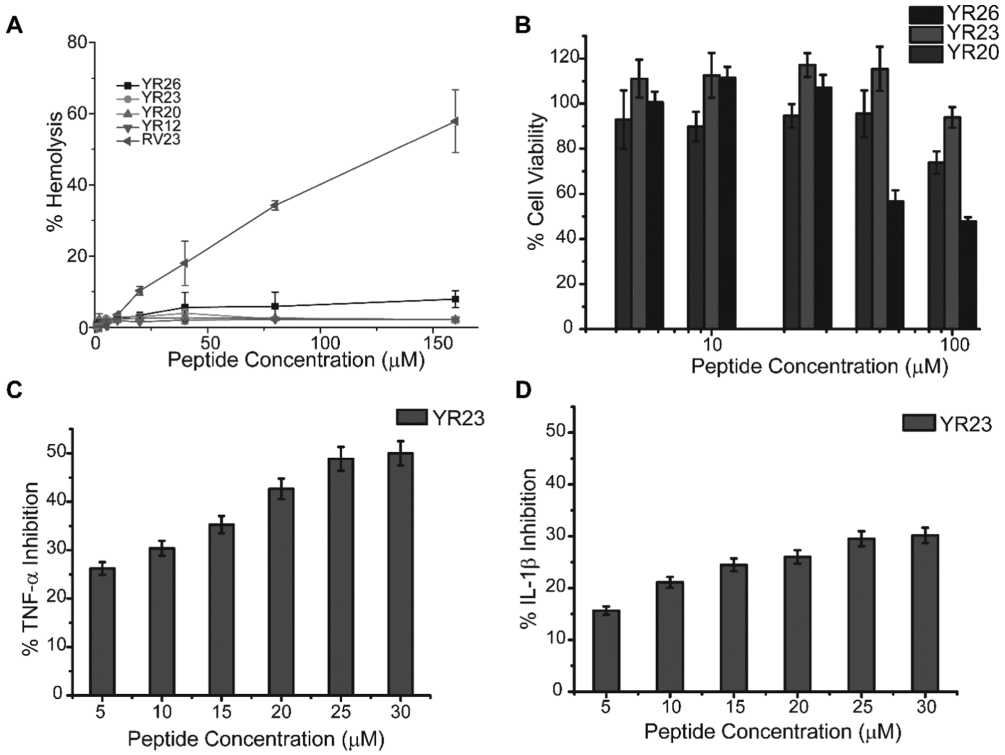

Figure 2. Furin prodomain-derived antibacterial peptides in human RBC lysis, mouse fibroblast cell NIH3T3 viability, and cytokine release from human THP-1 cell line. (A) Estimated % lysis of RBC as a function of concentrations of YR26, YR23, YR20, YR12, and RV23 peptides. (B) Peptides dose-dependent viability of mouse fibroblast cells. (C, D) Dose-dependent inhibition of (C) TNF-α and (D) IL-1β secretion by the YR23 peptide from LPS-induced THP-1 cells.

aliphatic and aromatic amino acids. Also, previous NMR structures revealed that the prodomain of furin assumed discretely folded helical conformations across several segments in 2,2,2-trifluoroethanol/water solution.[48,49] Such sequences and structural characteristics are also usually observed in membrane active AMPs. The C-terminus of the prodomain of furin is highly cationic and hydrophobic, therefore, we constructed overlapping peptide fragments, of various lengths, 15−35 residues, and examined antimicrobial activity (Figure 1 and Table 1). However, all five peptides, derived from the C-terminus were found to be largely inactive, minimum inhibitory concentration (MIC) > 100 μM, against representative Gram-negative and Gram-positive strains (Table 1). An N-terminal-derived peptide fragment, QF35, was also mostly inactive, except for *Escherichia coli*, MIC ∼ 20 μM (Table 1). To further map the internal sequence of the prodomain, two overlapping peptide fragments, RV23 and YR26, were obtained (Figure 1). The RV23 peptide did not delineate antibacterial activity except for *E. coli* (Table 1). Remarkably, the YR26 peptide fragment demonstrated growth inhibition against all of the bacterial strains with low MIC values (Table 1). To further determine sequence−activity correlations, several deletion analogs, from the C-terminus, of the active fragment YR26 were examined (Figure 1 and Table 2). The last three amino acids, QLR, of YR26 were found to be dispensable toward antibacterial activity (Table 2). The YR23 peptide demonstrated MIC values similar to the parent YR26 peptide (Tables 1 and 2). Furthermore, YR26 and YR23 peptides demonstrated growth inhibition against MRSA-resistant *S. aureus* and *S. epidermis* (Table 2). Peptide YR20, obtained from a further deletion of three residues of YR23, showed somewhat higher MIC values, in comparison to YR26 and YR23 peptides (Table 2). Further deletion of the three residues has yielded a largely inactive peptide, YH17 (Table 2). Interestingly, the more truncated variants, peptides YL14 and YR12 demonstrated improved activity profiles compared to the YH17 peptide fragment (Table 2).

DOI: 10.1021/acsomega.8b01876
ACS Omega 2018, 3, 14650−14664

Hemolysis and Fibroblast Cell Toxicity of the Prodomain-Derived AMPs. AMPs can be hemolytic and toxic to mammalian cells which would impede therapeutic development.[55,56] The effect of the antibacterial YR26, YR23, and YR20 peptides in the lysis of human red blood cells (RBCs) and their toxicity towards mouse fibroblast cells were examined (Figure 2, panels A and B). Figure 2A shows percentage hemolysis as a function of concentrations of prodomain-derived peptides. All three peptides demonstrated remarkably low hemolytic activity. At the highest concentration, 160 μM, of peptides, YR26 delineated an estimated hemolysis of 7.65%, whereas YR23 and YR20 peptides showed even lower hemolysis (Figure 2A). Interestingly, a high hemolytic activity, ∼71%, was estimated for the inactive peptide RV23 (Figure 2A). The viability of mouse NIHT3T cells was estimated by standard 3-(4,5-dimethylthiazol-2-yl)-2,5-diphenyltetrazolium bromide (MTT) assays at 5, 10, 25, 50, and 100 μM concentrations of peptides (Figure 2B). Cell viability was largely unaffected in the presence of the YR23 peptide even at the highest peptide concentration. Cell viability appeared to be somewhat decreased for YR26 and YR20 peptides at concentrations of 50 and 100 μM (Figure 2B). Note, MIC values of most active YR26 and YR23 peptides were estimated to be in the range of 2−6 μM (Table 2). Therefore, low hemolytic and high cell viability of the prodomain-derived AMPs demonstrate their therapeutic potential. In particular, hemolytic activity and cytotoxicity were deduced to be the lowest for the YR23 peptide.

Inhibition of TNF-α and IL-1β Cytokine Release from THP-1 Cells. Due to the lower cytotoxicity, the YR23 peptide was selected to examine inflammatory activity using the human monocytic cell line, THP-1. Enzyme-linked immunosorbent assays were performed to estimate the secreted TNF-α and IL-1β at graded concentrations of the YR23 peptide from LPS-treated THP-1 cells. To determine percentage inhibition, cytokines were also measured in the supernatant of cell culture in the absence and presence of LPS. As seen, YR23 demonstrated a dose-dependent inhibition of TNF-α and IL-β secretion from LPS-induced THP-1 cell lines (Figure 2, panels C and D). There was a gradual increase in the inhibition of TNF-α from 28 to 50% (Figure 2C) and IL-1β from 15 to 30% (Figure 2D) at 5 μM to 30 μM concentrations of the YR23 peptide. Therefore, the prodomain-derived peptide fragment YR23 retains the ability of suppressing the release of cytokines from human THP-1 cell line.

Disruption of Outer Membrane Permeability and Surface Charge Neutralization of *E. coli* Cells. We examined perturbation of the outer membrane and ζ-potential by the prodomain-derived peptides. *N*-Phenyl-1-naphthylamine (NPN), a fluorescent probe, is excluded from membrane interactions due to the permeability barrier of the outer membrane. Disruption of the outer membrane, caused by membrane active agents, allows NPN to interact with membrane lipids leading to an enhanced fluorescence emission. In separate experiments, NPN fluorescence emission spectra were obtained in *E. coli* cell solutions upon addition of various concentrations, ranging from 0 to 5 μM, of YR26, YR23, YR20, and YR12 peptides at a fixed probe concentration. Figure 3A shows the emission intensity (λ_{max} ∼ 410 nm) of NPN at different doses of peptides. Clearly, inclusion of the active peptides YR26 and YR23 into NPN *E. coli* cell solutions has caused a marked increase in the fluorescence intensity of the probe. The fluorescence intensity

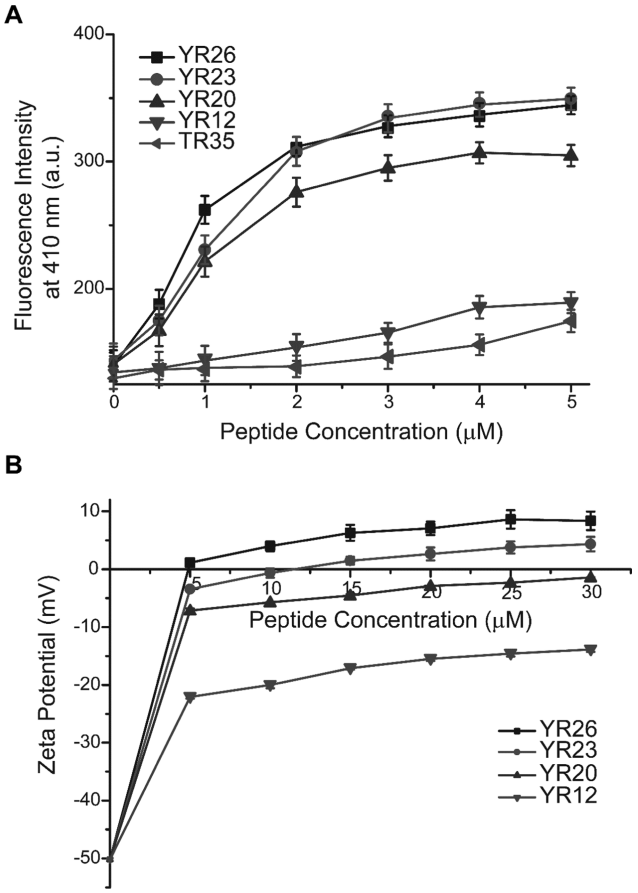

Figure 3. Prodomain-derived antibacterial peptides disrupted the outer membrane and neutralized the surface charge of *E. coli* cells. (A) Outer membrane permeability assay using NPN as a fluorescence probe. Increase in fluorescence intensity by the antibacterial peptides, YR26, YR23, and YR20 indicated their efficacy to permeabilize the outer cell membrane. (B) The ζ-potential of *E. coli* cells in the presence of varying concentrations of furin prodomain-derived peptides.

of NPN steadily increased from 0.5 to 2 μM peptide concentrations and attained a plateau beyond 3 μM concentration for both the peptides (Figure 3A). A somewhat lower change in fluorescence of NPN was observed upon addition of the YR20 peptide compared to YR26 and YR23. By contrast, only limited fluorescence enhancement of the probe was observed for the YR12 peptide (Figure 3A).

Towards bacterial cell killing, cationic AMPs can neutralize the negatively charged cell membrane which is thought to be important for membranolytic activity. Modes of membrane interactions of the prodomain-derived peptides were further investigated by measuring the ζ-potential of *E. coli* cell solutions. A predominantly negative ζ-potential, ∼−50 mV, of *E. coli* cells arises from phosphate and carboxylate of the outer membrane lipids and LPS molecules (Figure 3B).[57,58] The ζ-potential of *E. coli* cell solutions was measured at various concentrations, 5−30 μM, of YR26, YR23, YR20, and YR12 peptides in independent experiments (Figure 3B). As evident, the YR26 and YR23 peptides demonstrated the most efficient neutralization of the bacterial surface charge (Figure 3B). Even at 5 μM concentration of peptides, the bacterial surface charge became neutral for YR26 and remained low negative for YR23 (Figure 3B). The ζ-potential values were estimated to be

DOI: 10.1021/acsomega.8b01876
ACS Omega 2018, 3, 14650−14664

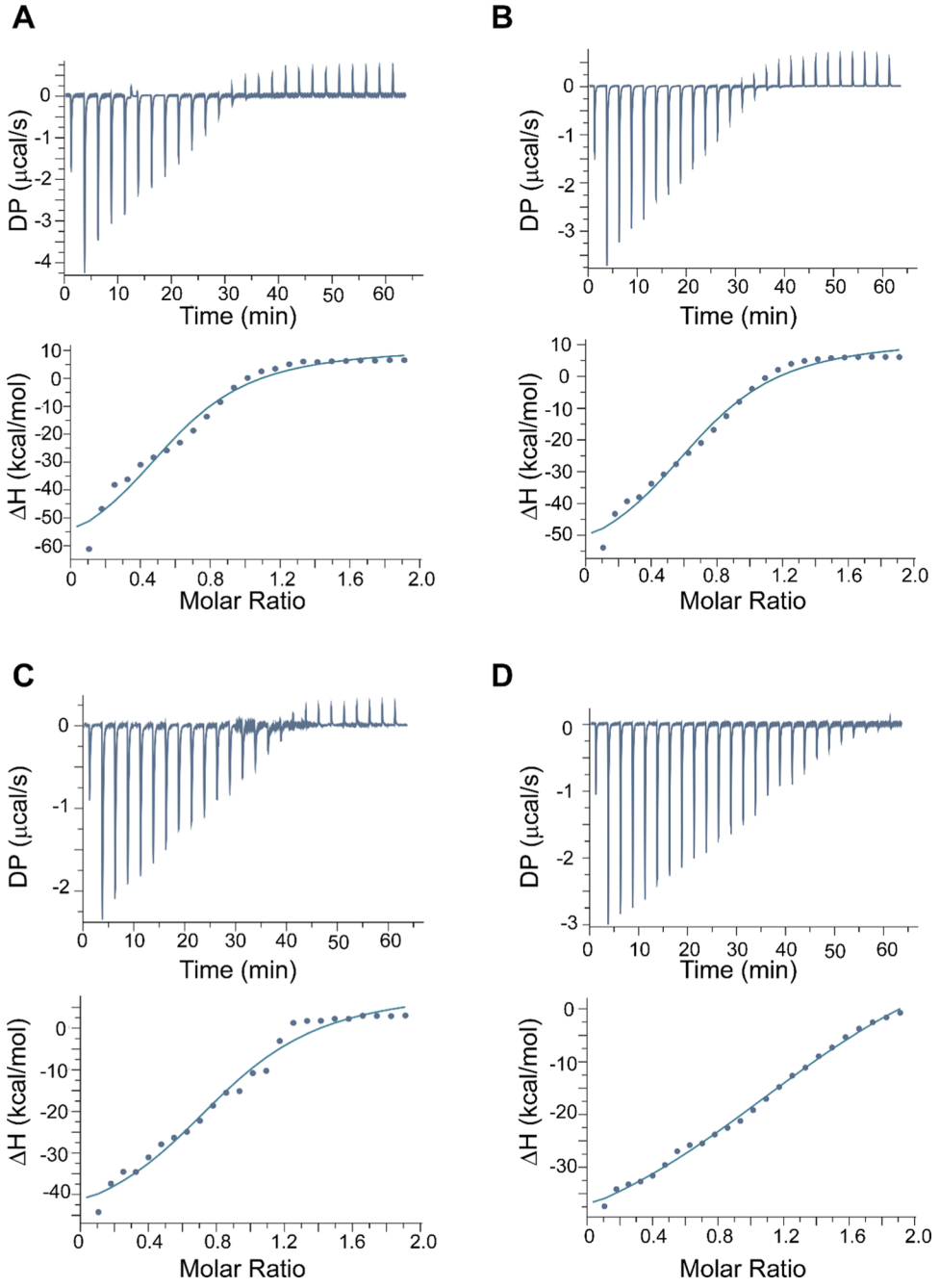

Figure 4. Binding energetics of prodomain-derived peptides in complex LPS. ITC thermograms of peptides (A) YR26, (B) YR23, (C) YR20, and (D) YR12. The top panel of each ITC profile shows titrated peaks as a function of time and the lower panel represents the integrated heat value of each titration point. ITC experiments were carried out in sodium phosphate buffer, pH 7.0, 37 °C.

positive, +5 to +10 mV, at the higher doses of YR26 and YR23 peptides. As seen, the ability of the YR20 peptide to completely neutralize the surface charge was lower compared to YR26 and YR23 peptides (Figure 3B). By contrast, the short peptide YR12 delineated a poor charge neutralization activity. Therefore, antibacterial peptides, YR26 and YR23, could efficiently disrupt the permeability barrier of the outer membrane and neutralize the surface charge of Gram-negative bacteria. Whereas, the YR20 peptide appeared to be moderately active in membrane permeabilization and charge neutralization. By contrast, the less active YR12 peptide delineated a limited outer membrane permeabilization and surface charge neutralization.

Interactions of the Prodomain-Derived Peptides with LPS. LPS is the major constituent of the outer leaflet of the outer membrane of Gram-negative bacteria.[59,60] Cationic AMPs might interact with the negatively charged LPS-outer membrane for disrupting the membrane barrier.[21,61] Interactions of LPS and prodomain peptides were investigated by using multiple methods, including isothermal titration calorimetry (ITC), intrinsic Trp fluorescence of peptides, and dynamic light scattering (DLS). Figure 4 (panels A–D) shows ITC thermograms of the interactions of the prodomain peptides with LPS. The ITC data revealed that peptide/LPS interactions were driven by exothermic processes as evident from the negative heat or downward positions of ITC thermal

DOI: 10.1021/acsomega.8b01876
ACS Omega 2018, 3, 14650−14664

profiles. Table 3 summarizes binding affinity and thermodynamic parameters of prodomain peptides/LPS interactions.

Table 3. Thermodynamic Interactions between LPS and Prodomain Peptides Determined from ITC[a]

peptide	K_d (μM)	ΔH (kcal/mol)	ΔG (kcal/mol)	$-T\Delta S$ (kcal/mol)
YR26	6.98	−80	−7.32	72.7
YR23	7.09	−74	−7.31	66.7
YR20	7.65	−59.5	−7.26	52.2
YR12	19.00	−69	−6.70	62.3

[a]Experiments were carried out in sodium phosphate buffer, pH 7 at 37 °C.

The active peptides YR26, YR23, and also YR20 interacted with LPS delineating comparable K_d values. By contrast, the YR12 peptide of limited antibacterial activity interacted with LPS with appreciably low affinity (Table 3). Furthermore, intrinsic Trp fluorescence emission spectra of the prodomain-derived peptides were obtained at various concentrations of LPS. Binding of the prodomain antimicrobial peptides with LPS caused a blue-shift of the emission maxima of Trp residue and concomitant quenching of the emission intensity with increased concentrations of LPS (Figure 5A). The observed blue shift in fluorescence emission maxima suggested that the Trp residue of the prodomain antimicrobial peptides inserts into the hydrophobic milieu of LPS. Notably, YR26, YR23, and YR20 showed higher λ_{max} shift compared to the YR12 peptide. The ability of the prodomain antimicrobial peptides to perturb LPS structural organization was probed by DLS experiments. In solution, LPS forms large micelle aggregates that could be disassembled into smaller sizes upon binding with cationic AMPs or LPS neutralizing proteins.[62−64] The size of the LPS micelle was estimated in free solution and at various molar ratios, 1:1, 1:2, and 1:4, of peptides (Figure 5, panels C−E). As one would expect, the active peptides YR26, YR23, and YR20 demonstrated large reduction of aggregated/micelle sizes of LPS in a dose-dependent manner. The free LPS micelles showed an average diameter (R_H) of 958 nm, whereas 214 and 217 nm R_H values were estimated in the complex with YR26 and YR23 peptides at a 1:1 ratio, respectively. The less active peptide YR12 delineated disaggregation of LPS micelle sizes to a lower extent, an R_H of 664 nm was estimated at a 1:1 ratio. Collectively, these aforementioned results demonstrated that the antibacterial prodomain peptides YR26, YR23, and YR20 could efficiently interact and destabilize LPS-aggregated structures.

Entrapped Dye Leakage and Interactions of the Prodomain Peptides with Liposomes. Lipid vesicles, entrapped with 5-carboxyfluorescein (CF) dye, purely consisted of either zwitterionic lipid 1-palmitoyl-2-oleoyl-*sn*-glycero-3-phosphocholine (POPC) or as a mixture of anionic lipids POPC/2-oleoyl-1-pamlitoyl-*sn*-glyecro-3-glycerol (POPG) (3:1) were prepared and the ability of the prodomain peptides to release the entrapped dye was investigated. The extent of the CF dye release from POPC/POPG (3:1) and POPC lipid vesicles was estimated as a function of different doses of prodomain peptides (Figure 6, panels A and B). As evident, the active peptides, YR26 and YR23, had caused leakage of the CF dye from the POPC/POPG (3:1) vesicles (Figure 6A). By contrast, prodomain peptides were unable to induce the release of the entrapped dye from POPC vesicles (Figure 6B).

To correlate lipid binding specificity, we investigated the binding and perturbation of the liposomes with prodomain-derived peptides using intrinsic Trp fluorescence (Supporting Information Figure S1) and DLS experiments (Figure 6, panels C−F, Supporting Information Figure S2). As seen, Trp emission maxima of YR26 and YR23 antibacterial peptides experienced a marked blue shift and a high quantum yield in emission intensity with increasing concentrations of POPC/POPG large unilamellar vesicles (LUVs), suggesting the incorporation of the fluorophore in the nonpolar environment of the liposomes (Supporting Information Figure S1). Interestingly, the YR12 peptide also showed interactions with POPC/POPG LUVs similar to the active peptides YR26 and YR23 (Supporting Information Figure S1). By contrast, there were no discernable changes in the Trp emission maxima for any of the peptides in POPC LUVs, implying limited interactions with zwitterionic lipids (Supporting Information Figure S1).

Binding interactions of the prodomain peptides with lipid vesicles were further investigated by assessing size distribution by using DLS studies. There were no significant changes in the mean diameter of zwitterionic POPC liposomes even at 4-fold higher concentrations of the peptides (Supporting Information Figure S2 and Table S1). These observations suggested that the prodomain-derived antibacterial peptides were unable to impart any structural perturbation toward zwitterionic liposomes. Remarkably, inclusions of YR26, YR23, and YR20 peptides into solutions containing POPC/POPG (3:1) lipid vesicles yielded a large increase in the size of the liposome (Figure 6, panels C−F and Table S2). The mean diameter of the liposomes was estimated to be increased as a function of peptide concentrations (Figure 6 and Table S1). Notably, the increase of the liposome size was limited and observed only at higher molar ratios for the YR12 peptide (Table S2). Therefore, lipid vesicle studies established that the antibacterial prodomain peptides selectively bind to the liposome containing the negatively charged phospholipids. The binding has induced leakage of dye from the liposomes and fusion of liposomes.

NMR Structure and Backbone Mobility of YR26 Peptide. The atomic-resolution structure and ^{15}N backbone dynamics of the long active peptide YR26 were determined in a negatively charged SDS micelle using ^{1}H and ^{15}N NMR spectroscopy. For heteronuclear NMR experiments, YR26 was recombinantly expressed, ^{15}N isotope labeled and purified from KSI fusion protein (see Materials and Methods). Sequence-specific resonance assignments of residues were achieved by analyses of two-dimensional $^{1}H-^{1}H$ TOCSY, NOESY, and ^{15}N edited three-dimensional (3D) NOESY-HSQC experiments. Figure 7A shows the $^{15}N-^{1}H$ HSQC spectrum of YR26 showing cross-peak assignments. Analyses of $^{1}H-^{1}H$ two-dimensional (2D) NOESY and 3D NOESY-HSQC spectra revealed sequential and medium range (i to i + 2, i + 3, i + 4) NOEs involving backbone/backbone, backbone/sidechain, and sidechain/sidechain. Figure 7B summarizes the number of NOEs observed for residues of YR26 in SDS micelles. Residue W42 delineated as many as 19 NOEs followed by residues L51 and H58 with 17 and 16 NOEs, respectively (Figure 7B). Notably, the medium range NOEs could not be ascertained for residues P53-R54-P55-R56 at the C-terminal half of YR26. An ensemble of the micelle-bound structure of YR26 was determined, by using CYANA, from 191 NOE driven distance and 40 backbone dihedral

DOI: 10.1021/acsomega.8b01876
ACS Omega 2018, 3, 14650−14664

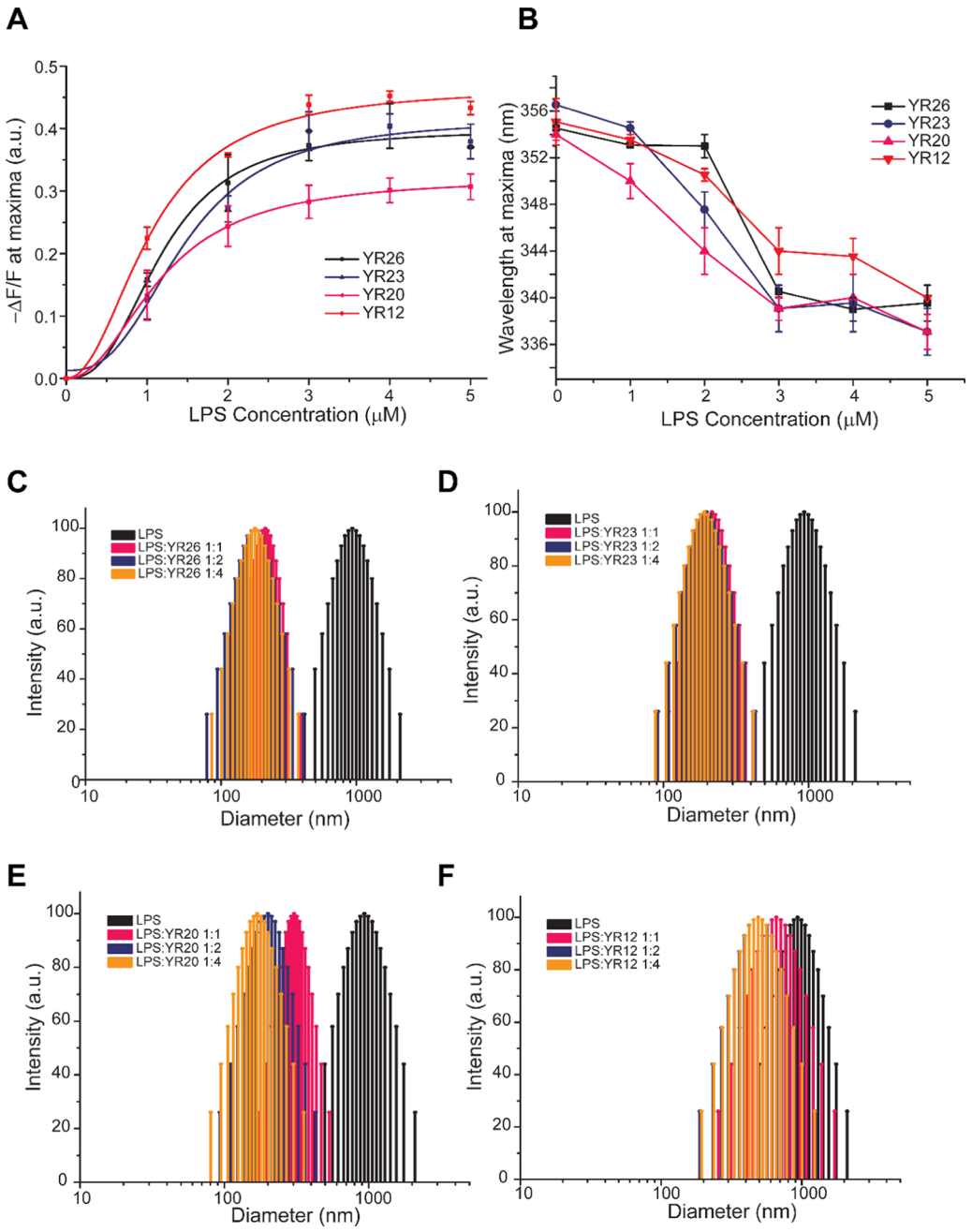

Figure 5. Interactions and perturbation of LPS-induced by prodomain-derived antibacterial peptides. Intrinsic Trp fluorescence experiments of YR26, YR23, YR20, and YR12 peptides as a function of concentrations of LPS. (A) Changes in fluorescence intensity at the emission maxima and (B) changes in emission wavelength (λ_{max}). (C−F) Bar diagrams show particle size distribution of LPS, estimated from DLS experiments, in free solutions and at different molar ratios of peptides (C) YR26, (D) YR23, (E) YR20, and (F) YR12.

angle (ϕ, ψ) constrains (Figure 8A). Structural parameters and statistics are listed in the Supporting Information Table S3. The root-mean-square deviation values of backbone atoms (Cα, C′, N) and all heavy atoms were estimated to be 0.27 and 1.7 Å, respectively (Table S3). The YR26 prodomain peptide assumes a helix-turn-helix structure in SDS micelle. The N-terminus of the molecule, comprising residues Y39-S52, folds into a long helix. This is followed by a sharp turn consisting of residues P53-P56 and a short C-terminal helix encompassing residues R57-Q62 (Figure 8B). The N-terminus helix appears to be slightly deviated from an idealized geometry at residue H43, showing a backbone dihedral angle of $\phi \sim -110°$, $\psi \sim -38°$. There are potential sidechain packing interactions among aromatic residues H40/W42/H43 and residues Y38/F41 (Figure 8B). The helix-turn-helix structure demonstrates multiple cationic patches throughout the topology (Figure 8C). Remarkably, a large cationic patch can be realized by the sidechain of residues, K48, R49, R55, R57, R60, and R63, from the N- and C-termini helices (Figure 8C). The cationic patch could be further complemented by basic sidechains of residues H54 and H58 (Figure 8C). A short cationic patch is sustained by the sidechains of residues R44/H43/H40 at the N-terminus half (Figure 8C).

The backbone motional characteristics of all nonprolyl residues, except for residue R63, of YR26 were determined by measuring ^{15}N spin relaxation rates, longitudinal relaxation

DOI: 10.1021/acsomega.8b01876
ACS Omega 2018, 3, 14650−14664

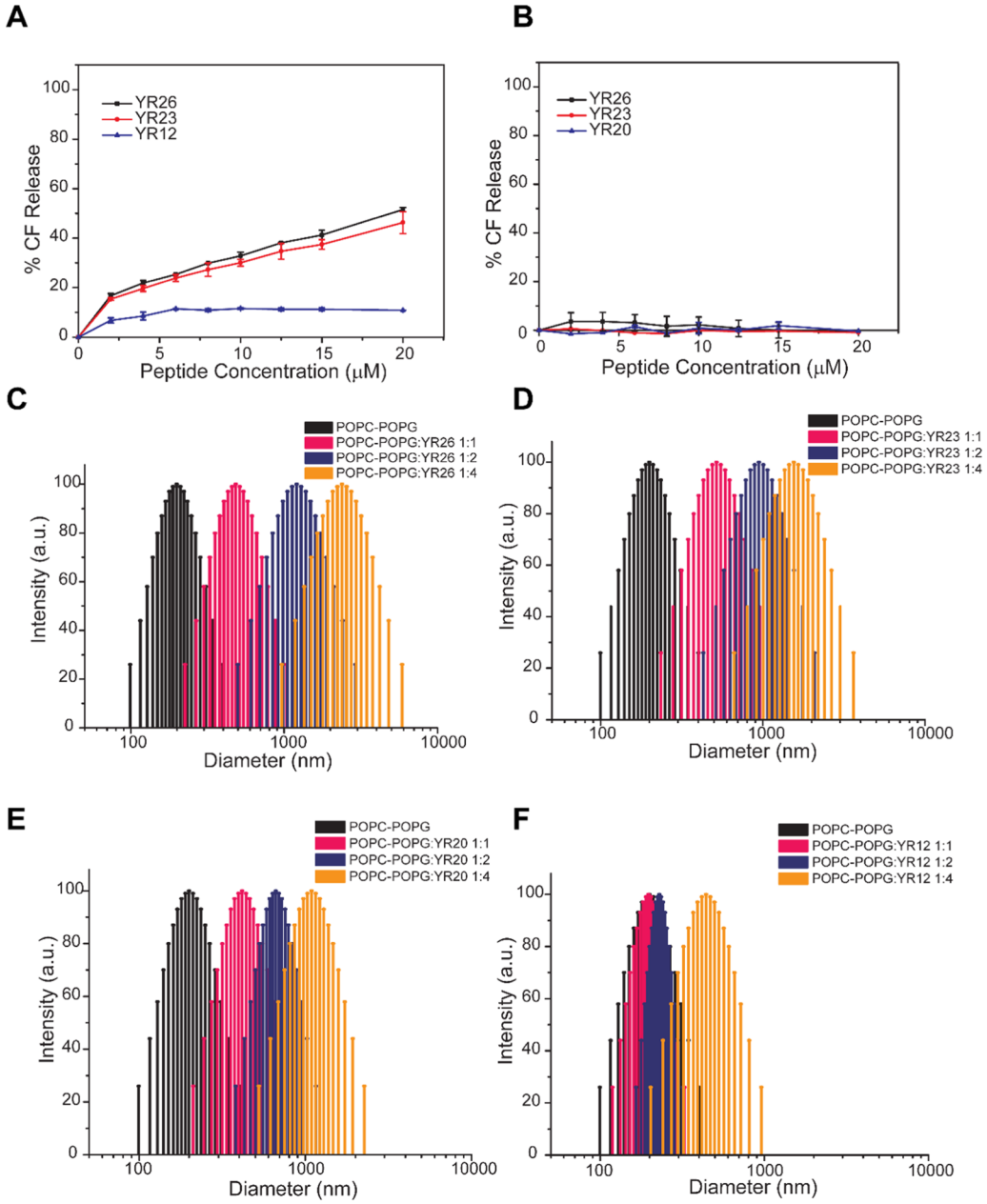

Figure 6. Binding of prodomain-derived antibacterial peptides to lipid vesicles. Estimation of CF dye release as a function of concentrations of YR26, YR23, and YR12 peptides from (A) POPC−POPG vesicles and (B) POPC vesicles. (C−F) Bar diagrams show the particle size distribution of POPC−POPG vesicles, estimated from DLS experiments, in free solutions and at different molar ratios of peptides (C) YR26, (D) YR23, (E) YR20, and (F) YR12.

(R_1), transverse relaxation (R_2), and heteronuclear NOE. The fast motion of the N−H bond vector, at picosecond and nanosecond time scale, is sensitive to these relaxation parameters. As seen, both R_1 and R_2 values were found to be largely uniform for almost all residues of YR26 (Figure 9, panels A and B). Residues Y39 and Q62, located near the termini, showed somewhat lower R_2 values compared to other residues. High heteronuclear NOE values (0.45−0.62) were estimated for most of the residues of YR26 suggesting that the residues are conformationally rigid (Figure 9C). Residues Arg49 and Ser52 delineated comparatively lower NOE values (0.38−0.41) indicating that the region may be relatively mobile. Residues Tyr39 and Gln62 near the termini showed much lower NOE values of 0.17 and 0.24, respectively. This suggests that the residues near the terminal are flexible, as expected.

DISCUSSION

Cell-Selective Antimicrobial and Anti-inflammatory Peptides from the Prodomain of Furin. Discovery, characterization, and mode of action of new cell-selective AMPs would be valuable to strengthen the pool of antimicrobial compounds. Several methods are employed to identify AMPs including screening of peptide libraries, computer-aided design and de novo design.[13,65−69] Notably, a recent study, aimed to screen antimicrobial peptides from a massive pool of random sequences, demonstrated that only 1.7% of the sequence space could be active.[13] On the basis of

DOI: 10.1021/acsomega.8b01876
ACS Omega 2018, 3, 14650−14664

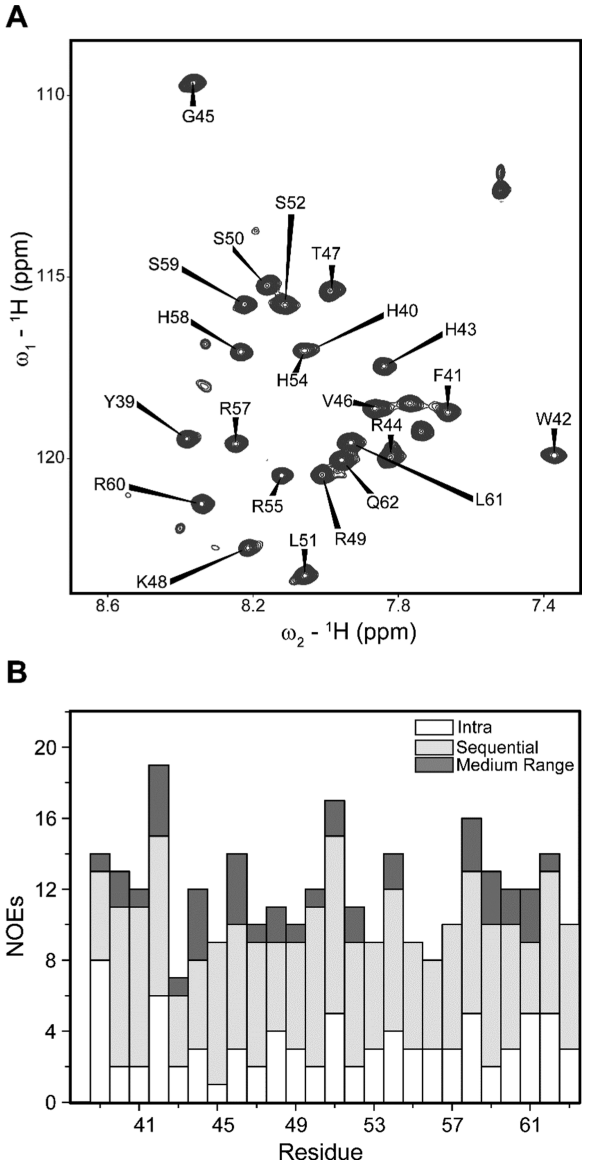

Figure 7. NMR analyses of the antibacterial YR26 peptide fragment of prodomain of furin in SDS micelles. (A) The $^{15}N-^{1}H$ HSQC spectrum of ^{15}N-labeled YR26 peptide showing assignment of individual residue. (B) Bar diagram delineates the number of NOE contacts for each residue of YR26 peptide.

the cationicity and hydrophobicity, we surmised that the prodomain of furin may yield antimicrobial peptides. Toward this, we designed several overlapping synthetic peptide fragments from the N and C-termini of prodomain of furin for screening antibacterial activity. As seen, many of the prodomain peptide fragments were largely devoid of antibacterial activity with MIC > 100 μM (Figure 1 and Table 1). Remarkably, an internal peptide fragment, residues Y38-R62 or YR26, demonstrated potent broad-spectrum activity, MIC ranges between 2 and 4 μM, against several bacterial strains (Table 2). The N-terminus of YR26 consists of a stretch of aromatic residues Y38YHFWH43 whereas the C-terminal region is more variable with cationic, polar, and Pro residues (Figure 1). Deletion of either three or six residues at the C-terminus, yielding peptides YR23 and YR20, respectively, did not largely affect antibacterial activity. However, YR20 delineated slightly higher MICs (Table 2). The antibacterial peptides, YR26, YR23, and YR20, were found to be poorly hemolytic and also displayed low toxicity to fibroblast cells. Notably, in comparison to other prodomain peptide fragments, the YR23 peptide not only retained a broad-spectrum antibacterial activity but also demonstrated least toxicity toward RBC and fibroblast cells. Furthermore, in a set of enzyme-linked immunosorbent assay assays, YR23 efficiently blocked LPS or endotoxin-induced release of cytokines, TNF-α and IL-1β from THP-1 cell line. The inhibition of cytokine release indicated that the YR23 peptide can ameliorate toxicity of LPS.

Furin Prodomain-Derived Antibacterial Peptides Interacted with LPS and Disrupted LPS-Outer membrane. The outer-membrane of Gram-negative bacteria establishes a permeability barrier due to a high content of LPS molecules located at the outer leaflet of the bilayer.[70,71] Hydrophobic antibiotics and antibacterial agents could be excluded by the LPS-outer membrane.[70,71] The LPS-mediated barrier appears to be causing significant difficulty in drug development against Gram-negative pathogens.[6,7,22] Notably, during septic shock syndrome caused by LPS or endotoxin in blood stream, over production of the tissue damaging cytokines contribute to the multiple organ failures and fatal outcome.[72,73] In the absence of therapeutics, there are ongoing efforts to develop drugs against sepsis.[74,75] Cationic AMPs and LPS interacting molecules are considered as vital leads for the antisepsis drug development.[61,69] The antibacterial peptides YR26, YR23, and YR20 permeabilized LPS-outer membrane and neutralized surface charge of bacterial cells (Figure 3). Binding of the prodomain-derived peptides to LPS, estimated by ITC experiments, revealed that the active peptides bind to LPS with higher affinity compared to peptide YR12 which displayed a high MIC (Table 3). Moreover, the exothermic binding observed in the ITC thermograms supported prevalent ionic and/or polar interactions of the antibacterial cationic peptides with the negatively charged LPS (Figure 4 and Table 3). The ionic interactions are considered to be the first step in anchoring AMPs to the bacterial cell wall components.[20−22] Intrinsic Trp fluorescence revealed that the Trp residues of YR26, YR23, and YR20 peptides inserted into the lipidic milieu of LPS. Furthermore, as evident from DLS studies, binding of the prodomain antibacterial peptides to LPS has yielded significant disruption of the higher order assemblies of LPS into smaller aggregated structures (Figure 5). By contrast, the YR12 peptide, delineating lower antibacterial activity, was found to be limited in cell permeabilization and LPS structural perturbation. Therefore, LPS-outer membrane interactions and perturbation of LPS structures would be critical in the antibacterial activity of AMPs.

Antibacterial Prodomain Peptides Interacted with Negatively Charged Lipid Vesicles Causing Dye Leakage and Aggregations. Lipid vesicles or liposomes are widely used as a close mimic of the plasma membrane of cells. The inner membrane of a bacterial cell contains more negatively charged PG phospholipids, whereas the plasma membrane of mammalian or human cells are rich in zwitterionic phospholipids. Prodomain peptides interacted specifically with the negatively charged POPC/POPG vesicles compared to vesicles consisting of zwitterionic POPC lipids (Figure 6). These data correlate well with the limited ability of the antibacterial peptides to lyse human RBC and low toxicity to fibroblast cells. Notably, active peptides, YR26, YR23, and YR20, and also the less active peptide, YR12, were found to be

DOI: 10.1021/acsomega.8b01876
ACS Omega 2018, 3, 14650−14664

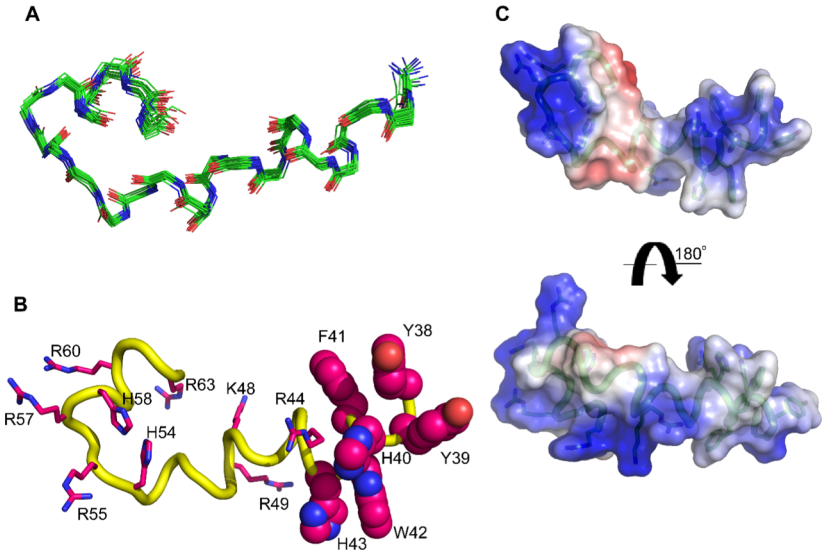

Figure 8. Atomic-resolution structure of the antibacterial YR26 peptide bound to SDS micelle. (A) Superposition of backbone atoms of 20 lowest energy structures of YR26 calculated from CYANA. The pdb coordinates of the structures of YR26 have been deposited to pdb data bank, accession number 6A8Y. (B) Ribbon representation of a selected structure of YR26 showing a helix-turn-helix fold. The sidechains of N-terminal aromatic residues are shown as space-fill whereas sidechains of basic residues are shown as sticks. (C) The electrostatic surface potential surface of YR26 in two different orientations highlighting cationic patches.

inserted into POPC/POPG vesicles. However, only binding of the antibacterial peptides, YR26 and YR23 to POPC/POPG vesicles had promoted the release of the entrapped CF dye and transformation of liposomes into large aggregated structures. It is worth mentioning that the leakage of the entrapped dye from liposomes are usually observed by pore forming AMPs.[20−24] However, the fusion of liposomes induced by cationic AMPs had been delineated for mouse defesine cryptdin-4, Lfcin B, and MSI 103.[76−78] Such liposome fusion perhaps indicates an efficient insertion of the AMPs into bilayer and perturbation of packing interactions among the lipid molecules.[78]

Novel Helix-Turn-Helix Structure of YR26 Prodomain Peptide YR26 in SDS Micelle. The atomic-resolution structure and backbone dynamics of the YR26 peptide were elucidated in a solution of SDS micelle by NMR spectroscopy. Note that the negatively charged SDS micelles are frequently used as a bacterial membrane mimic for the structural determination of AMPs. Heteronuclear NOEs demonstrated that most of the residues of YR26, except for few at the termini, are motionally rigid in the micelle-bound state (Figure 9). In SDS micelle, YR26 folded into a compact helix-turn-helix structure. In particular, the two helices, long N-terminal and short C-terminal, are orientated in an antiparallel manner and are connected by a tight turn maintained by multiple Pro residues (Figure 8). The helix-turn-helix structure of YR26 appears to be lacking a clear disposition of nonpolar and cationic faces which are frequently observed in micelle-bound structures of amphipathic AMPs.[22−24] However, the tertiary fold of the YR26 peptide in the SDS micelle is sustained by the isolated patches of aromatic and cationic surfaces (Figure 8). Strikingly, in the bipartite helical structure, the N-terminal helix are predominantly involved in the aromatic cluster, residues H40/W42/H43 and Y38/F41, whereas only fewer residues, R44, K48, and R49 are found in the cationic patch. The fold back of the C-terminal helix maintains most of the cationic surface of the structure of YR26 through residues R55, R57, R60, and R63 (Figure 8). The atomic-resolution structure of YR26 and biophysical experiments may provide mechanistic insights into bacterial membrane interactions and permeabilization. The cationic patches of the helix-turn-helix structure are likely to establish ionic interactions with the negatively charged phosphates of the LPS-outer membrane and also with the plasma membrane of bacteria. The ionic interactions between YR26 and the membrane appeared to be highly critical. Since, deletion of residues, including many cationic ones, of the C-terminal helix and loop, in analog YH17, drastically impaired antibacterial activity, we surmise that followed by membrane charge neutralization, aromatic and nonpolar residues of the helix-loop-helix structure would insert into the hydrophobic environment of the membrane. These interactions between membranes and prodomain peptide YR26 are likely to cause disruption of membrane packing that may lead to bacterial cell death.

In conclusion, the current work has defined human furin prodomain peptide fragments with a broad spectrum of antibacterial activity including MRSA-resistant *Staphylococcus* strains. The antibacterial peptides are extremely nonhemolytic, nontoxic to mammalian cells, and able to suppress tissue damaging cytokine release. As a mode of action, the prodomain peptides interacted specifically with negatively charged lipids including the LPS-outer membrane and disrupted bacterial membrane integrity. The atomic-resolution structure of YR26 obtained in SDS micelle described the potential membrane interacting cationic and aromatic surfaces. The antibacterial activity, atomic-resolution structure, and associated biophysical characteristics of the prodomain furin peptides can be further utilized for the development of cell-selective antimicrobial drugs and materials.

MATERIALS AND METHODS

Furin prodomain-derived peptides (95% pure) were purchased from Synpeptide Co. Ltd. (Shanghai, China). LPS from *E. coli* 0111:B4, MH broth, SDS, and fluorescent dyes, NPN and 6-carboxyfluorescein, were obtained from Sigma-Aldrich. Lipids such as POPC and POPG and the extruder used for the preparation of liposomes were procured from Avanti Polar

DOI: 10.1021/acsomega.8b01876
ACS Omega 2018, 3, 14650−14664

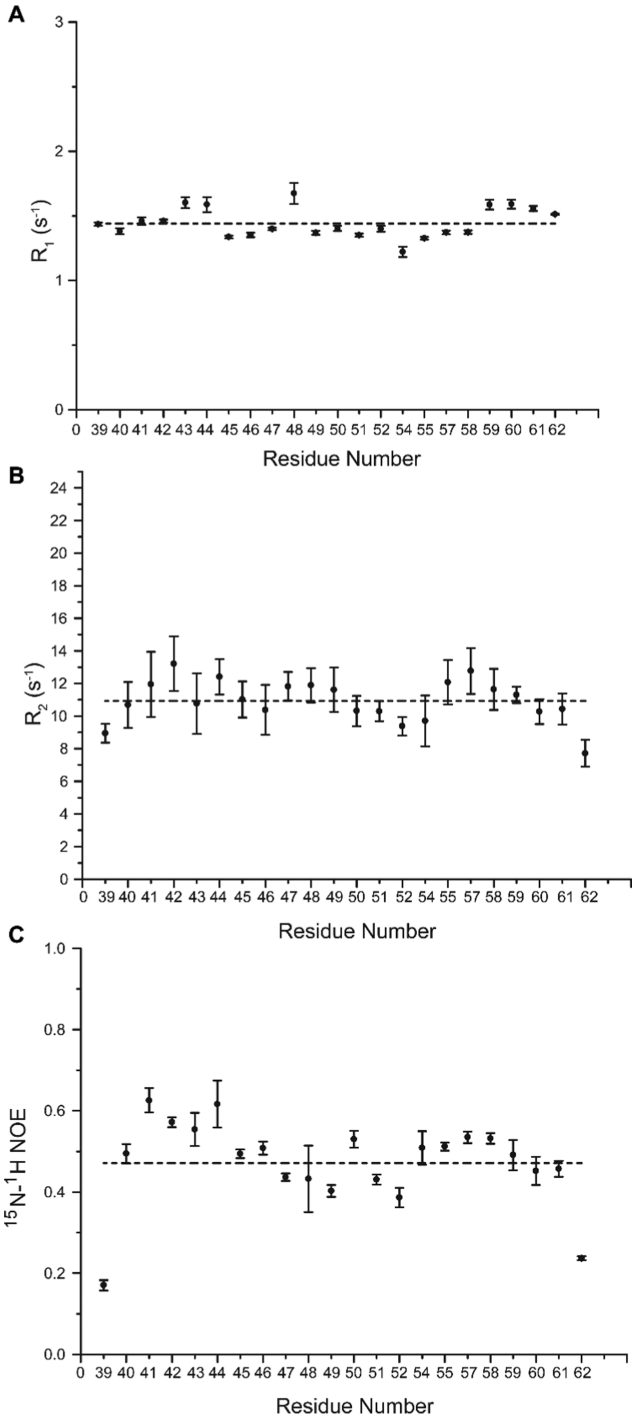

Figure 9. Backbone motional characteristics of YR26 in SDS micelle. (A) Longitudinal (R_1) relaxation rate of residues of YR26, with an average of 1.44 s^{-1}. (B) Transverse (R_2) relaxation rate of residues of YR26, with an average of 10.93 s^{-1}. (C) Heteronuclear NOEs of residues of YR26, with an average of 0.47. The dotted line in the plot indicates average values of R_1, R_2, and heteronuclear NOE.

lipids (Alabaster, AL). NMR reagents such as 2,2-dimethyl-2-silapentane 5-sulfonate sodium salt (DSS), D_2O, and SDS-d_{25} were purchased from Cambridge Isotope Laboratories, Inc (MA).

Minimum Inhibitory Concentration Measurement. Minimum inhibitory concentration (MIC) of prodomain peptides was measured using the broth dilution method. Mid-log phase cultures of four Gram-negative (*E. coli*, *P. aeruginosa* ATCC 27853, *K. Pneumoniae* ATCC 13883, *S. enterica* ATCC 14028), four Gram-positive (*B. subtilis*, *S. aureus* ATCC 25923, *S. pyogenes* ATCC 19615, *E. faecalis* ATCC 29212) bacteria, and two Gram-positive-resistant strains (*S. aureus* ATCC BAA-44 and *S. epidermis* ATCC 51625) were diluted in MHB to a final concentration of 5×10^5 CFU/mL. In a 96-well plate, 50 μL of peptides at final concentrations ranging from 30 to 0.25 μM were prepared and another 50 μL of the diluted bacterial solutions were added to each of the wells. The plate was incubated at 37 °C for 18 h. OD_{600} was measured and the minimum concentration at which there is complete inhibition of bacterial growth was recorded as the MIC of the peptide.

Hemolysis Assay. Fresh blood samples were taken from a healthy volunteer. The erythrocytes were washed with phosphate-buffered saline (PBS) (10 mM sodium phosphate buffer, 150 mM NaCl, pH 7) and 5% blood solution was prepared in PBS. In a 96-well plate, 50 μL of varying concentrations of peptides were prepared. Another 50 μL of 5% blood solution was added to each well. The plate was incubated for 1 h at 37 °C. The plate was centrifuged and the OD_{540} of the supernatant was measured. 1% triton-X was taken as a positive control and PBS was taken as a negative control. % hemolysis was calculated as: $\%\ \text{hemolysis} = \frac{\text{OD} - \text{OD}_{\text{negative}}}{\text{OD}_{\text{positive}} - \text{OD}_{\text{negative}}} \times 100$, where, OD: OD_{540} for any well $OD_{negative}$: OD_{540} for negative control $OD_{positive}$: OD_{540} for positive control

Cytotoxicity Test. NIH3T3 cell line was used to test the toxicity of the furin peptides towards mammalian cells. 10 000 cells were added per well in a 96-well plate and the plates were incubated overnight at 37 °C and 5% CO_2. After 24 h, media was removed and 100 μL of the desired concentration of peptides were added into fresh media. The plates were incubated for 4 h at 37 °C and 5% CO_2. The media was further replaced and 10 μL of MTT was added into each well followed by incubation for 4 h at 37 °C and 5% CO_2. Finally, the media was removed from every well and 100 μL of dimethyl sulfoxide was added to solubilize the crystals. The plates were incubated for 10 min. Each well was mixed thoroughly and OD was taken at 540 nm. For a negative control, no peptide was added and for positive control, no cells were added. % cell viability was calculated as: $\%\ \text{cell viability} = \frac{\text{OD}_{\text{negative}} - \text{OD}}{\text{OD}_{\text{negative}} - \text{OD}_{\text{positive}}} \times 100$, where, OD: OD_{540} for any well, $OD_{negative}$: OD_{540} for negative control, $OD_{positive}$: OD_{540} for positive control.

Cytokine Release Assays. Enzyme-linked immunosorbent assays were performed to estimate the secreted TNF-α and IL-1β in LPS-treated THP-1 cells in the presence of YR23 peptide after 4−12 h of incubation, as described elsewhere.[79] Cytokines in culture supernatant of untreated and LPS-treated cells were taken as minimum and maximum to determine percentage inhibition by YR23. The concentrations of TNF-α and IL-1β in the samples were estimated using human enzyme-linked immunosorbent assay kits for TNF-α (BD Biosciences cat. no. 555212) and IL-1β (BD Biosciences cat. no. 557953) according to the manufacturers' protocol. All experiments were repeated thrice and the average values of the cytokine concentrations were reported.

Outer Membrane Permeabilization Assay. The ability of the peptides to permeabilize the outer membrane was examined using the 1-*N*-phenylnaphthylamine (NPN) dye. *E.*

DOI: 10.1021/acsomega.8b01876
ACS Omega 2018, 3, 14650−14664

coli cells were grown to mid-log phase and were diluted to OD_{600} of 0.5 in 10 mM phosphate buffer, pH 7.0. 10 μM of NPN was added to the cells and basal fluorescence was recorded. This was followed by the addition of increasing concentrations of peptides and recording the emission spectra. Excitation wavelength was set as 350 nm and emission wavelength was recorded from 390 to 450 nm. The fluorescence measurements were carried out on a Cary Eclipse fluorescence spectrophotometer (Varian Inc) equipped with dual monochromators. Finally, the fluorescence intensity at maxima was estimated to examine the effect of the peptides on the outer membrane of the *E. coli* cells.

ζ-Potential Measurement. Mid-log phase *E. coli* were diluted to an OD_{600} of 0.2 in LB media. The ζ-potential of the bacterial cells was first measured in disposable zeta cells with gold electrodes. This was followed by adding increasing concentrations of peptides and measuring the ζ-potential. For each data point, 3 measurements of 100 runs each were carried out. The experiments were carried out on a zeta sizer Nano ZS (Malvern Instruments, Worcestershire, U.K.) equipped with a 633 nm He laser.

Isothermal Titration Calorimetry. Interactions of prodomain-derived antimicrobial peptides with LPS were studied using a microcal ITC 200 calorimeter. In the sample cell, 50 μM LPS in 10 mM phosphate buffer, pH 7 was loaded cell. 500 μM peptide stock was loaded in the syringe. The reference cell was filled with buffer and the stirring speed was set at 900 rpm. 25 injections of 1.5 μL peptides were made into the sample cell at 37 °C. A single-site binding model in Microcal PEAQ-ITC analysis software was used to fit the raw data to obtain the association constant (K_a) and enthalpy change (ΔH). Dissociation constant (K_d), Gibbs free energy (ΔG), and entropy change ($T\Delta S$) were calculated as: $K_d = 1/K_a$, $\Delta G = -RT \ln K_a$, $T\Delta S = \Delta H - \Delta G$.

Preparation of Liposomes. Bacterial cell mimicking POPC−POPG (3:1) liposomes and mammalian cell mimicking POPC liposomes were prepared to study peptide interactions. Dry weights of the appropriate lipids were measured in glass vials. Chloroform and methanol in the ratio of 3:1 was added to the vials to dissolve the lipids. The solvent was then evaporated under a stream of nitrogen gas. This leads to the formation of a thin film on the sides of the vials. The vials were then freeze dried for 2 h to completely remove any trace of the solvent. The film was then dissolved in 10 mM phosphate buffer, pH 7. The mixture was sonicated in a water bath for 30 min. The liposomes were made unilamellar by extruding the lipid through 100 nm membranes. The lamellarity of the liposomes was confirmed by analyzing their particle size by a dynamic light scattering technique. In the case of carboxyfluorescein (CF) entrapped liposomes, the film was dissolved in 10 mM phosphate buffer consisting of 70 mM CF. After extrusion, the unbound CF was separated from the CF-bound liposomes using a PD-10 desalting column.

Intrinsic Tryptophan Fluorescence Experiments. Basal fluorescence of the furin prodomain-derived peptides was measured by exciting peptides at 280 nm and recording the emission spectra from 300 to 400 nm. Change in the wavelength of emission intensity maxima was observed by the addition of increasing concentrations of LPS, POPC, and POPC−POPG liposomes. The fluorescence measurement was carried out in a Cary Eclipse fluorescence spectrophotometer using a 0.1 cm path length quartz cuvette.

Particle Size Analysis by Dynamic Light Scattering. Ability of the furin prodomain-derived AMPs to perturb liposomes was examined by analyzing the particle size of 1 μM POPC−POPG and POPC liposomes in the presence of increasing peptide concentrations. The mean diameter of free liposomes was first determined in 10 mM phosphate buffer, pH 7, using a dynamic light scattering instrument (Brookhaven Instruments Corp., Holtsville, NY). DLS measurements were then made for liposome:peptide ratios of 1:1, 1:2, and 1:4. The scattering data was analyzed using the particle sizing software provided with the instrument.

Carboxyfluorescein Leakage Assay. Membrane disruption ability of the furin peptides was determined by examining the release of carboxyfluorescein dye from CF-bound liposomes using the Cary Eclipse fluorescence spectrophotometer (Varian Inc). Basal fluorescence of the CF-bound liposomes was measured by exciting the vesicles at 495 nm and recording the emission fluorescence from 500 to 550 nm. Fluorescence emission spectra in the presence of increasing peptide concentration was also recorded. Change in emission intensity at maxima was then plotted against peptide concentration to examine the CF leakage in the presence of AMPs. The measurements were carried out using a 0.1 cm path length quartz cuvette.

Recombinant Expression and Purification of Isotope-Labeled YR26 Peptide Fragment. A synthetic gene of YR26, from Shanghai ShineGene Molecular Biotech, Inc, was cloned as a fusion protein in a pET14b vector containing hydrophobic KSI at the N-terminus. The pET14b vector contains six His-tag at the N-terminus for affinity purification. An Asn-Pro sequence was introduced between KSI and hydrophilic YR26 for chemical cleavage by formic acid. The recombinant plasmid (containing ampicillin resistance) was transformed into Rosetta *E. coli* cells (having chloramphenicol resistance). A single isolated colony was picked and cultured in LB medium with ampicillin (100 μg/mL) and chloramphenicol (32 μg/mL) overnight as a starter culture. Seed culture was transformed into 1L M9 media (containing ampicillin and chloramphenicol) in a 1:100 ratio by volume and was allowed to grow in a shaker incubator at 37 °C and 180 rpm for 6−7 h till its OD_{600} reached 0.6−0.8. The M9 media used consisted of ^{15}N ammonium chloride, necessary for ^{15}N labeling. The culture was then induced with 1 mM IPTG and was allowed to grow overnight at 37 °C and 180 rpm. The cells were harvested at 7000 rpm. Expression was checked using SDS-polyacrylamide gel electrophoresis gel electrophoresis. As the fusion protein is localized to inclusion bodies, protein purification was carried out in denaturing conditions (8 M urea). The cells were resuspended in binding buffer (8 M urea, 50 mM phosphate buffer, 300 mM NaCl), pH 8.0 and the mixture was incubated for 1 h while shaking at room temperature. The cells were then lysed by sonication. To eliminate cell debris, the translucent cell suspension was centrifuged at 15 000 rpm for 30 min at 4 °C. The supernatant containing the fusion protein was then loaded on the Nickel-NTA column (QIAGEN) and eluted using 8 M urea buffer containing 500 mM imidazole. Eluent containing pure protein was kept for dialysis against water for 36−48 h to remove urea and salts. The dialyzed mixture was then treated with 50% formic acid at 45−50 °C for 24 h in the dark. Formic acid cleaves the D−P bond and separates the ^{15}N-YR26 from KSI tag. Formic acid was removed using a rotary evaporator and the obtained film was redissolved in water. KSI being very

DOI: 10.1021/acsomega.8b01876
ACS Omega 2018, 3, 14650−14664

hydrophobic, precipitated out leaving behind a solution of ^{15}N YR26. The peptide was further purified using high-performance liquid chromatography and the major peak was confirmed by matrix-assisted laser desorption ionization time-of-flight and NMR.

NMR Experiments for Furin Prodomain-Derived YR26. All the NMR spectra were recorded on a Bruker DRX 600 spectrometer, equipped with a cryo-probe and pulse field gradients. Data acquisition and processing were performed with topspin software running on Linux workstation. To determine the structure of YR26 in the presence of SDS micelles, 0.3 mM peptides and 200 mM SDS in aqueous solution containing 10% D_2O at pH 5 were used to acquire 2D ^{1}H−^{1}H TOCSY and NOESY spectra at 298 K. Mixing times of 80 ms for TOCSY and 150 ms for NOESY were used. 2,2-Dimethyl-2-silapentane 5-sulfonate sodium salt (DSS) was used as an internal reference for chemical shift. NOESY experiments were performed with 400 increments in t1 and 64 transients. The WATERGATE procedure was used for water signal suppression. A total of 2 K data points was used in t2 and NMR data was analyzed in the Sparky (T. D. Goddard and D. G. Kneller, University of California, San Francisco, CA) program. Three-dimensional (3D) ^{1}H−^{15}N−^{1}H NOESY experiment was performed with 128 increments in t1 and 48 increments in t2. A total of 2 K data points were used in t3. Synthetic unlabeled YR26 was used to acquire the ^{13}C−^{1}H HSQC (natural abundance) spectrum in 100% D_2O at 298 K. 0.4 mM YR26 and 200 mM SDS were used for the experiment with 1024 increments in t1 and 56 transients. ^{15}N−^{1}H HSQC experiment was conducted for 0.44 mM ^{15}N YR26 and 220 mM SDS at 298 K, pH 5. The experiment was performed with 96 increments in t1 and 8 transients. ^{15}N−^{1}H heteronuclear NOE relaxation experiment conducted with 128 increments in t1 and 8 transients. The spectrum was split into saturated and unsaturated spectra of ^{1}H resonances. Heteronuclear ^{15}N−^{1}H NOEs were determined as the ratio of the peak intensities with and without proton saturation. The ^{15}N longitudinal (R_1) and transverse (R_2) relaxation rate constants were determined by collecting a time series of ^{15}N−^{1}H HSQC spectra with sensitivity enhancement. For R_1 measurements, the spectra were acquired at relaxation delays of 0.2, 0.6, 0.9, 1.2, 1.5, 2.0, and 2.5 s, with repeat experiment at 1.5 s for error estimation. For R_2 measurements, the data were recorded at 10, 30, 50, 70, 90, and 110 ms, with repeat experiment at 70 ms for error measurement. For relaxation experiments, 2 K data points were used in t2 with 90 increments in t1. The relaxation constants were determined by fitting the cross-peak intensities to a monoexponential function.

Structure Determination of YR26 in SDS Micelle. The 3D structure of YR26 in the presence of SDS was calculated using the CYANA program. Distance restraints were estimated from two-dimensional NOESY spectra on the basis of NOE intensities. Strong, medium, and weak NOEs were translated to upper bound distance limits of 2.5, 3.5, and 5.0 Å, respectively. Hα chemical shift deviation of individual amino acids from the NOESY spectrum, ^{13}C chemical shift deviation from the ^{13}C−^{1}H HSQC spectrum and ^{15}N chemical shift deviation from the ^{15}N−^{1}H HSQC spectrum were incorporated in SHIFTY to calculate dihedral angle constraint. Out of 100 structures calculated, 20 lowest energy structures were kept for further analysis. PROCHECK was used to produce the Ramachandran plot, which was in turn used to validate the structures calculated.

■ ASSOCIATED CONTENT

Supporting Information

The Supporting Information is available free of charge on the ACS Publications website at DOI: 10.1021/acsomega.8b01876.

pdb coordinates of the structures (PDB)

Intrinsic tryptophan fluorescence of the peptides YR26, YR23, YR20, and YR12 (Figure S1); particle size of POPC liposomes, determined from DLS experiments (Figure S2); particle size analysis of zwitterionic POPC liposomes (Table S1); particle size analysis of POPC−POPG liposomes (Table S2); summary of structural statistics of 20 low energy structures of the prodomain peptide YR26 bound to anionic SDS micelles (Table S3) (PDF)

■ AUTHOR INFORMATION

Corresponding Author

*E-mail: surajit@ntu.edu.sg. Fax: 65-6791-3856.

ORCID

Surajit Bhattacharjya: 0000-0001-7015-1937

Notes

The authors declare no competing financial interest.

■ ACKNOWLEDGMENTS

This work is supported by the Ministry of Education (Grants ARC18/13, RG140/17), Singapore.

■ REFERENCES

(1) O'Neill, J. Tackling Drug-Resistant Infections Globally: Final Report and Recommendations. *Review on Antimicrobial Resistance*, 2016.

(2) Lohner, K.; Staudegger, E. Are we on the threshold of the post-antibiotic era. *Development of Novel Antimicrobial Agents: Emerging Strategies*; Horizon Press, 2001; pp 1−15.

(3) Reardon, S. Antibiotic resistance sweeping developing world: bacteria are increasingly dodging extermination as drug availability outpaces regulation. *Nature* **2014**, *509*, 141−143.

(4) Control, C. F. D. *Prevention, Antibiotic resistance threats in the United States, 2013. Centres for Disease Control and Prevention*; US Department of Health and Human Services, 2013.

(5) Boucher, H. W.; Talbot, G. H.; Bradley, J. S.; Edwards, J. E.; Gilbert, D.; Rice, L. B.; Scheld, M.; Spellberg, B.; Bartlett, J. Bad bugs, no drugs: no ESKAPE! An update from the Infectious Diseases Society of America. *Clin. Infect. Dis.* **2009**, *48*, 1−12.

(6) Higgins, P. G.; Dammhayn, C.; Hackel, M.; Seifert, H. Global spread of carbapenem-resistant *Acinetobacter baumannii*. *J. Antimicrob. Chemother.* **2010**, *65*, 233−238.

(7) Lewis, K. Platforms for antibiotic discovery. *Nat. Rev. Drug Discovery* **2013**, *12*, 371.

(8) Clatworthy, A. E.; Pierson, E.; Hung, D. T. Targeting virulence: a new paradigm for antimicrobial therapy. *Nat. Chem. Biol.* **2007**, *3*, 541.

(9) Zasloff, M. Antimicrobial peptides of multicellular organisms. *Nature* **2002**, *415*, 389−395.

(10) Hancock, R. E.; Sahl, H. G. Antimicrobial and host-defense peptides as new anti-infective therapeutic strategies. *Nat. Biotechnol.* **2006**, *24*, 1551−1557.

(11) Kang, H.-K.; Kim, C.; Seo, C. H.; Park, Y. The therapeutic applications of antimicrobial peptides (AMPs): a patent review. *J. Microbiol.* **2017**, *55*, 1−12.

(12) Park, S.-C.; Park, Y.; Hahm, K.-S. The role of antimicrobial peptides in preventing multidrug-resistant bacterial infections and biofilm formation. *Int. J. Mol. Sci.* **2011**, *12*, 5971−5992.

DOI: 10.1021/acsomega.8b01876
ACS Omega 2018, 3, 14650−14664

(13) Tucker, A. T.; Leonard, S. P.; DuBois, C. D.; Knauf, G. A.; Cunningham, A. L.; Wilke, C. O.; Trent, M. S.; Davies, B. W. Discovery of Next-Generation Antimicrobials through Bacterial Self-Screening of Surface-Displayed Peptide Libraries. *Cell* **2018**, *172*, 618−628.
(14) Kumar, P.; Kizhakkedathu, J. N.; Straus, S. K. Antimicrobial Peptides: Diversity, Mechanism of Action and Strategies to Improve the Activity and Biocompatibility In Vivo. *Biomolecules* **2018**, *8*, 4.
(15) Tam, J. P.; Wang, S.; Wong, K. H.; Tan, W. L. Antimicrobial peptides from plants. *Pharmaceuticals* **2015**, *8*, 711−757.
(16) Hilchie, A. L.; Wuerth, K.; Hancock, R. E. Immune modulation by multifaceted cationic host defense (antimicrobial) peptides. *Nat. Chem. Biol.* **2013**, *9*, 761−768.
(17) Wang, G. *Antimicrobial Peptides: Discovery, Design and Novel Therapeutic Strategies*; Cabi, 2017.
(18) Ganz, T. Defensins: antimicrobial peptides of innate immunity. *Nat. Rev. Immunol.* **2003**, *3*, 710−720.
(19) Agerberth, B.; Gunne, H.; Odeberg, J.; Kogner, P.; Boman, H. G.; Gudmundsson, G. H. FALL-39, a putative human peptide antibiotic, is cysteine-free and expressed in bone marrow and testis. *Proc. Natl. Acad. Sci. U.S.A.* **1995**, *92*, 195−199.
(20) Shai, Y. Mode of action of membrane active antimicrobial peptides. *Biopolymers* **2002**, *66*, 236−248.
(21) Bhattacharjya, S.; Ramamoorthy, A. Multifunctional host defense peptides: functional and mechanistic insights from NMR structures of potent antimicrobial peptides. *FEBS J.* **2009**, *276*, 6465−6473.
(22) Yeaman, M. R.; Yount, N. Y. Mechanisms of antimicrobial peptide action and resistance. *Pharmacol. Rev.* **2003**, *55*, 27−55.
(23) Nguyen, L. T.; Haney, E. F.; Vogel, H. J. The expanding scope of antimicrobial peptide structures and their modes of action. *Trends Biotechnol.* **2011**, *29*, 464−472.
(24) Brogden, K. A. Antimicrobial peptides: pore formers or metabolic inhibitors in bacteria? *Nat. Rev. Microbiol.* **2005**, *3*, 238−250.
(25) Marquette, A.; Bechinger, B. Biophysical investigations elucidating the mechanisms of action of antimicrobial peptides and their synergism. *Biomolecules* **2018**, *8*, 18.
(26) Polikanov, Y. S.; Aleksashin, N. A.; Beckert, B.; Wilson, D. N. The mechanisms of action of ribosome-targeting peptide antibiotics. *Front. Mol. Biosci.* **2018**, *5*, 48.
(27) Scocchi, M.; Mardirossian, M.; Runti, G.; Benincasa, M. Non-membrane permeabilizing modes of action of antimicrobial peptides on bacteria. *Curr. Top. Med. Chem.* **2016**, *16*, 76−88.
(28) Alexander, J. L.; Thompson, Z.; Cowan, J. Antimicrobial metallopeptides. *ACS Chem. Biol.* **2018**, *13*, 844−853.
(29) Wang, G. Human antimicrobial peptides and proteins. *Pharmaceuticals* **2014**, *7*, 545−594.
(30) Dürr, U. H.; Sudheendra, U.; Ramamoorthy, A. LL-37, the only human member of the cathelicidin family of antimicrobial peptides. *Biochim. Biophys. Acta, Biomembr.* **2006**, *1758*, 1408−1425.
(31) Wang, G.; Li, X.; Wang, Z. APD3: the antimicrobial peptide database as a tool for research and education. *Nucleic Acids Res.* **2016**, *44*, D1087−D1093.
(32) Mathew, B.; Nagaraj, R. Variations in the interaction of human defensins with *Escherichia coli*: possible implications in bacterial killing. *PLoS One* **2017**, *12*, No. e0175858.
(33) Wang, C.; Shen, M.; Gohain, N.; Tolbert, W. D.; Chen, F.; Zhang, N.; Yang, K.; Wang, A.; Su, Y.; Cheng, T.; et al. Design of a potent antibiotic peptide based on the active region of human defensin 5. *J. Med. Chem.* **2015**, *58*, 3083−3093.
(34) Du, H.; Puri, S.; McCall, A.; Norris, H. L.; Russo, T.; Edgerton, M. Human salivary protein histatin 5 has potent bactericidal activity against ESKAPE pathogens. *Front. Cell. Infect. Microbiol.* **2017**, *7*, 41.
(35) Song, C.; Weichbrodt, C.; Salnikov, E. S.; Dynowski, M.; Forsberg, B. O.; Bechinger, B.; Steinem, C.; de Groot, B. L.; Zachariae, U.; Zeth, K. Crystal structure and functional mechanism of a human antimicrobial membrane channel. *Proc. Natl. Acad. Sci. U.S.A.* **2013**, *110*, 4586−4591.
(36) Paulmann, M.; Arnold, T.; Linke, D.; Özdirekcan, S.; Kopp, A.; Gutsmann, T.; Kalbacher, H.; Wanke, I.; Schuenemann, V. J.; Habeck, M.; et al. Structure-activity analysis of the dermcidin-derived peptide DCD-1L, an anionic antimicrobial peptide present in human sweat. *J. Biol. Chem.* **2012**, *287*, 8434−8443.
(37) Harder, J.; Schröder, J.-M. RNase 7, a novel innate immune defense antimicrobial protein of healthy human skin. *J. Biol. Chem.* **2002**, *277*, 46779−46784.
(38) Pulido, D.; Moussaoui, M.; Andreu, D.; Nogués, M. V.; Torrent, M.; Boix, E. Antimicrobial action and cell agglutination by the eosinophil cationic protein are modulated by the cell wall lipopolysaccharide structure. *Antimicrob. Agents Chemother.* **2012**, *56*, 2378−2385.
(39) Ibrahim, H. R.; Thomas, U.; Pellegrini, A. A helix-loop-helix peptide at the upper lip of the active site cleft of lysozyme confers potent antimicrobial activity with membrane permeabilization action. *J. Biol. Chem.* **2001**, *276*, 43767−43774.
(40) Hunter, H. N.; Jing, W.; Schibli, D. J.; Trinh, T.; Park, I. Y.; Kim, S. C.; Vogel, H. J. The interactions of antimicrobial peptides derived from lysozyme with model membrane systems. *Biochim. Biophys. Acta, Biomembr.* **2005**, *1668*, 175−189.
(41) Park, C. B.; Kim, M. S.; Kim, S. C. A Novel Antimicrobial peptide from bufo bufo gargarizans. *Biochem. Biophys. Res. Commun.* **1996**, *218*, 408−413.
(42) Pane, K.; Sgambati, V.; Zanfardino, A.; Smaldone, G.; Cafaro, V.; Angrisano, T.; Pedone, E.; Di Gaetano, S.; Capasso, D.; Haney, E. F.; et al. A new cryptic cationic antimicrobial peptide from human apolipoprotein E with antibacterial activity and immunomodulatory effects on human cells. *FEBS J.* **2016**, *283*, 2115−2131.
(43) Papareddy, P.; Rydengård, V.; Pasupuleti, M.; Walse, B.; Mörgelin, M.; Chalupka, A.; Malmsten, M.; Schmidtchen, A. Proteolysis of human thrombin generates novel host defense peptides. *PLoS Pathog.* **2010**, *6*, No. e1000857.
(44) Kasetty, G.; Papareddy, P.; Kalle, M.; Rydengård, V.; Mörgelin, M.; Albiger, B.; Malmsten, M.; Schmidtchen, A. Structure-activity studies and therapeutic potential of host defense peptides of human thrombin. *Antimicrob. Agents Chemother.* **2011**, *55*, 2880−2890.
(45) Petrlova, J.; Hansen, F. C.; Van Der Plas, M. J.; Huber, R. G.; Mörgelin, M.; Malmsten, M.; Bond, P. J.; Schmidtchen, A. Aggregation of thrombin-derived C-terminal fragments as a previously undisclosed host defense mechanism. *Proc. Natl. Acad. Sci. U.S.A.* **2017**, *114*, E4213−E4222.
(46) Thomas, G. Furin at the cutting edge: from protein traffic to embryogenesis and disease. *Nat. Rev. Mol. Cell Biol.* **2002**, *3*, 753−766.
(47) Seidah, N. G.; Sadr, M. S.; Chrétien, M.; Mbikay, M. The multifaceted proprotein convertases: their unique, redundant, complementary, and opposite functions. *J. Biol. Chem.* **2013**, *288*, 21473−21481.
(48) Bhattacharjya, S.; Xu, P.; Xiang, H.; Chrétien, M.; Seidah, N. G.; Ni, F. pH-induced conformational transitions of a molten−globule−like state of the inhibitory prodomain of furin: Implications for zymogen activation. *Protein Sci.* **2001**, *10*, 934−942.
(49) Bhattacharjya, S.; Xu, P.; Wang, P.; Osborne, M. J.; Ni, F. Conformational analyses of a partially-folded bioactive prodomain of human furin. *Biopolymers* **2007**, *86*, 329−344.
(50) Yu, Y.; Lei, X.; Jiang, H.; Li, Z.; Creemers, J. W.; Zhang, M.; Qin, S.; Jin, W.; Jiang, X. C. Prodomain of furin promotes phospholipid transfer protein proteasomal degradation in hepatocytes. *J. Am. Heart Assoc.* **2018**, *7*, No. e008526.
(51) Benjannet, S.; Elagoz, A.; Wickham, L.; Mamarbachi, M.; Munzer, J. S.; Basak, A.; Lazure, C.; Cromlish, J. A.; Sisodia, S.; Checler, F.; et al. Post-translational processing of β-secretase (β-amyloid-converting enzyme) and its ectodomain shedding the pro- and transmembrane/cytosolic domains affect its cellular activity and amyloid-β production. *J. Biol. Chem.* **2001**, *276*, 10879−10887.
(52) Lei, X.; Basu, D.; Li, Z.; Zhang, M.; Rudic, R. D.; Jiang, X.-C.; Jin, W. Hepatic overexpression of the prodomain of furin lessens

DOI: 10.1021/acsomega.8b01876
ACS Omega 2018, 3, 14650−14664

progression of atherosclerosis and reduces vascular remodeling in response to injury. *Atherosclerosis* **2014**, *236*, 121−130.
(53) Scamuffa, N.; Sfaxi, F.; Ma, J.; Lalou, C.; Seidah, N.; Calvo, F.; Khatib, A.-M. Prodomain of the proprotein convertase subtilisin/kexin Furin (ppFurin) protects from tumor progression and metastasis. *Carcinogenesis* **2014**, *35*, 528−536.
(54) Bhattacharjya, S.; Xu, P.; Zhong, M.; Chrétien, M.; Seidah, N. G.; Ni, F. Inhibitory activity and structural characterization of a C-terminal peptide fragment derived from the prosegment of the proprotein convertase PC7. *Biochemistry* **2000**, *39*, 2868−2877.
(55) Gajski, G.; Domijan, A.-M.; Žegura, B.; Štern, A.; Gerić, M.; Jovanović, I. N.; Vrhovac, I.; Madunić, J.; Breljak, D.; Filipič, M.; Garaj-Vrhovac, V. Melittin induced cytogenetic damage, oxidative stress and changes in gene expression in human peripheral blood lymphocytes. *Toxicon* **2016**, *110*, 56−67.
(56) Mukherjee, I.; Ghosh, A.; Bhadury, P.; De, P. Side-chain amino acid-based cationic antibacterial polymers: investigating the morphological switching of a polymer-treated bacterial cell. *ACS Omega* **2017**, *2*, 1633−1644.
(57) Alves, C. S.; Melo, M. N.; Franquelim, H. G.; Ferre, R.; Planas, M.; Feliu, L.; Bardají, E.; Kowalczyk, W.; Andreu, D.; Santos, N. C.; et al. *Escherichia coli* cell surface perturbation and disruption induced by antimicrobial peptides BP100 and pepR. *J. Biol. Chem.* **2010**, *285*, 27536−27544.
(58) Saravanan, R.; Mohanram, H.; Joshi, M.; Domadia, P. N.; Torres, J.; Ruedl, C.; Bhattacharjya, S. Structure, activity and interactions of the cysteine deleted analog of tachyplesin-1 with lipopolysaccharide micelle: Mechanistic insights into outer-membrane permeabilization and endotoxin neutralization. *Biochim. Biophys. Acta, Biomembr.* **2012**, *1818*, 1613−1624.
(59) Raetz, C. R.; Whitfield, C. Lipopolysaccharide endotoxins. *Annu. Rev. Biochem.* **2002**, *71*, 635−700.
(60) Cronan, J. E. Bacterial membrane lipids: where do we stand? *Annu. Rev. Microbiol.* **2003**, *57*, 203−224.
(61) Bhattacharjya, S. NMR structures and interactions of antimicrobial peptides with lipopolysaccharide: connecting structures to functions. *Curr. Top. Med. Chem.* **2016**, *16*, 4−15.
(62) Mohanram, H.; Bhattacharjya, S. Resurrecting inactive antimicrobial peptides from the lipopolysaccharide trap. *Antimicrob. Agents Chemother.* **2014**, *58*, 1987−1996.
(63) Datta, A.; Ghosh, A.; Airoldi, C.; Sperandeo, P.; Mroue, K. H.; Jiménez-Barbero, J.; Kundu, P.; Ramamoorthy, A.; Bhunia, A. Antimicrobial peptides: insights into membrane permeabilization, lipopolysaccharide fragmentation and application in plant disease control. *Sci. Rep.* **2015**, *5*, No. 11951.
(64) Mangoni, M. L.; Epand, R. F.; Rosenfeld, Y.; Peleg, A.; Barra, D.; Epand, R. M.; Shai, Y. Lipopolysaccharide, a key molecule involved in the synergism between temporins in inhibiting bacterial growth and in endotoxin neutralization. *J. Biol. Chem.* **2008**, *283*, 22907−22917.
(65) Fjell, C. D.; Hiss, J. A.; Hancock, R. E.; Schneider, G. Designing antimicrobial peptides: form follows function. *Nat. Rev. Drug Discovery* **2011**, *11*, 37−51.
(66) Hilpert, K.; Volkmer-Engert, R.; Walter, T.; Hancock, R. E. High-throughput generation of small antibacterial peptides with improved activity. *Nat. Biotechnol.* **2005**, *23*, 1008−10012.
(67) Dou, X.; Zhu, X.; Wang, J.; Dong, N.; Shan, A. Novel design of heptad amphiphiles to enhance cell selectivity, salt resistance, antibiofilm properties and their membrane-disruptive mechanism. *J. Med. Chem.* **2017**, *60*, 2257−2270.
(68) Rathinakumar, R.; Walkenhorst, W. F.; Wimley, W. C. Broad specutrum antimicrobial peptides by rational combinatorial design and high throughput screening: the importance of interfacial activity. *J. Am. Chem. Soc.* **2009**, *131*, 7609−7617.
(69) Bhunia, A.; Mohanram, H.; Domadia, P. N.; Torres, J.; Bhattacharjya, S. Designed β-boomerang antiendotoxic and nntimicrobial peptides: structures and activties in lipopolysaccharide. *J. Biol. Chem.* **2009**, *284*, 21991−22004.
(70) Snyder, D. S.; McIntosh, T. J. The lipopolysaccharide barrier: correlation of antibiotic susceptibility with antibiotic permeability and fluorescent probe binding kinetics. *Biochemistry* **2000**, *39*, 11777−11787.
(71) Delcour, A. H. Outer membrane permeability and antibiotic resistance. *Biochim. Biophys. Acta, Proteins Proteomics* **2009**, *1794*, 808−816.
(72) Martin, G. S.; Mannino, D. M.; Eaton, S.; Moss, M. The epidemiology of sepsis in the United States from 1979 through 2000. *N. Engl. J. Med.* **2003**, *348*, 1546−1554.
(73) Cohen, J. The immunopathogenesis of sepsis. *Nature* **2002**, *420*, 885−891.
(74) Fink, M. P.; Warren, H. S. Strategies to improve drug development for sepsis. *Nat. Rev. Drug Discovery* **2014**, *13*, 741−758.
(75) Lehmann, C.; Sharawi, N.; Al-Banna, N.; Corbett, N.; Kuethe, J. W.; Caldwell, C. C. Novel approaches to the development of anti-sepsis drugs. *Expert Opin. Drug Discovery* **2014**, *9*, 523−531.
(76) Cummings, J. E.; Vanderlick, T. K. Aggregation and hemifusion of anionic vesicles induced by the antimicrobial peptide cryptdin-4. *Biochim. Biophys. Acta, Biomembr.* **2007**, *1768*, 1796−1804.
(77) Ulvatne, H.; Haukland, H.; Olsvik, Ø.; Vorland, L. Lactoferricin B causes depolarization of the cytoplasmic membrane of *Escherichia coli* ATCC 25922 and fusion of negatively charged liposomes. *FEBS Lett.* **2001**, *492*, 62−65.
(78) Wadhwani, P.; Reichert, J.; Bürck, J.; Ulrich, A. S. Antimicrobial and cell-penetrating peptides induce lipid vesicle fusion by folding and aggregation. *Eur. Biophys. J.* **2012**, *41*, 177−187.
(79) Harioudh, M. K.; Sahai, R.; Mitra, K.; Ghosh, J. K. A short non-cytotoxic antimicrobial peptide designed from Aβ29-40 adopts nanostructure and shows in vivo anti-endotoxin activity. *Chem. Commun.* **2017**, *53*, 13079−13082.

DOI: 10.1021/acsomega.8b01876
ACS Omega 2018, 3, 14650−14664